Nonequilibrium Modeling of Reactive Distillation: A Dusty Fluid Model for Heterogeneously Catalyzed Processes

Arnoud Higler,[†,§] R. Krishna,[‡] and Ross Taylor*[,†,§]

Department of Chemical Engineering, Clarkson University, CU Box 5705, Potsdam, New York 13699−5705, Department of Chemical Engineering, University of Amsterdam, Nieuwe Achtergracht 166, 1018 WV, Amsterdam, The Netherlands, and Department of Chemical Engineering, University of Twente, Postbus 217, 7500 AE, Enschede, The Netherlands

We have developed a nonequilibrium model for heterogeneous catalytic distillation in which we have explicitly taken into account simultaneous mass transfer and reaction inside the catalyst particle. This was done by using a finite difference approximation of the dusty fluid model. Calculations were done for a methyl *tert*-butyl ether (MTBE) column and a *tert*-amyl methyl ether (TAME) column. It was found that there are hardly any differences between a pseudohomogeneous nonequilibrium model and a dusty fluid nonequilibrium model, for the TAME process. The simulation results for the TAME process compare favorably with the experimental data of Mohl et al. (*Chem. Eng. Sci.* **1999**, *54*, 1029). For the MTBE process the pseudohomogeneous model predicts multiple steady states. However, the window of opportunity for multiple steady states seems to disappear entirely using the dusty fluid model. The explanation for the contrasting behavior of the TAME and MTBE processes has to do with the fact that the latter is significantly more sensitive to increased mass-transfer resistances.

1. Introduction

In many ways, reactive distillation (RD) represents an ideal chemical process, combining the key operations of most chemical processes—reaction and separation—in the same piece of equipment.[2] A reactive distillation column usually is split into three sections: A reactive section, in which the reactants are converted into products, and where, by means of distillation, the products are separated out of the reactive zone. The tasks of the rectifying and stripping sections depend on the boiling points of the reactants and products. If the product is the lowest boiling component in the process, the rectifying section is used for product purification and reactant recycle and the stripping section is used mainly for inert and byproduct removal as well as reactant recycle. If the product is the highest boiling component, the tasks of the rectifying and stripping sections are switched. The column internals could be trays or packing. Packed RD columns could be filled with structured sheet metal packing that has been treated to make the surface catalytically active so as to promote the desired chemical reactions.[3] A packed RD column could also be equipped with porous catalytic packing, either in the form of the traditional Raschig ring[4] or of the so-called "teabag" or "sandwich" type in which porous catalyst particles are confined within a wire mesh support.[5−7]

Mathematical models of several different levels of complexity for reactive distillation operations have been presented in the literature. The simpler models adopt an equilibrium stage approach with an equilibrium reaction.[8−10] Other equilibrium stage models incorporate finite reaction rates into the equation system for standard equilibrium models for distillation columns.[11−18] The more sophisticated nonequilibrium (NEQ) models take account of both finite reaction rates and finite interphase mass-transfer fluxes.[4,19−21]

In conventional distillation operations it suffices to take into consideration diffusion in the vapor and liquid phases.[22] The mass-transfer modeling usually is done using the rigorous Maxwell−Stefan theory.[23] RD operations may be more complicated in that additional mass-transfer resistances might need to be modeled. In columns packed with coated sheet metal packings we have diffusion to (and from) the active sheet metal surface. In dumped-ring-type and teabag-type packings the reaction takes place inside porous catalyst particles and, to be completely rigorous, we should model diffusion to and from the catalyst surface as well as diffusion and reaction inside the catalyst particles. It is modeling this latter type of heterogeneous catalytic distillation operation with which we shall be concerned in this paper.

Diffusion and reaction inside porous catalysts often is modeled using simple effective diffusivity models of the diffusion process and an effectiveness factor (a function of the Thiele modulus) to represent the effect of reaction.[24] In a pair of papers Sundmacher and Hoffmann[25,26] present a nonequilibrium model for heterogeneously catalyzed reactive distillation. For incorporation of the reaction rate, they have developed a mathematical model to analyze the interaction of the internal mass and heat transport with the microkinetics of the heterogeneous reaction. The coupled balance equations for transport and reaction are reduced to a single differential equation, for which solutions, depending on a generalized Thiele modulus and an effectiveness factor, are derived for three geometries. This

* To whom correspondence should be addressed. Telephone: 315-268-6652. Fax: 315-268-6654. E-mail: taylor@clarkson.edu.
[†] Clarkson University.
[‡] University of Amsterdam.
[§] University of Twente.

10.1021/ie990547q CCC: $19.00
Published on Web 04/04/2000

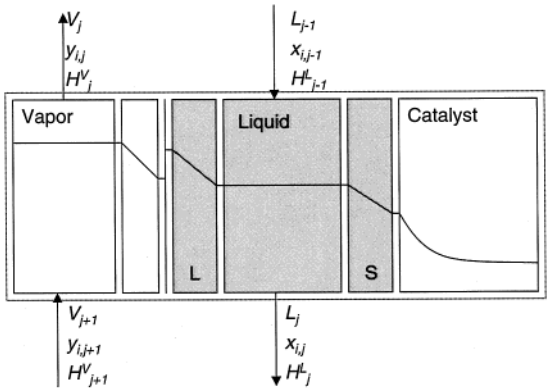

Figure 1. Schematic representation of the unit cell for a heterogeneous catalytic distillation model.

effectiveness factor is used in a pseudohomogeneous reaction rate expression in the liquid-phase mass balances.

In this paper we will use a more rigorous theory of diffusion (and reaction) inside porous catalysts: the "dusty fluid model".

2. Nonequilibrium Model

A detailed nonequilibrium cell model for a reactive distillation column with homogeneous and pseudohomogeneous reactions has been described by Higler et al.[20] Here, we will present only the changes to the nonequilibrium cell model equations required for a third phase—the porous catalyst.

A schematic diagram of the unit cell for a vapor−liquid-porous catalyst system is shown in Figure 1. It is assumed that the bulk of both vapor and liquid phases are ideally mixed and that the mass-transfer resistances are located in films near the vapor/liquid and liquid/solid interfaces. The liquid film at the vapor−liquid-phase boundary will be denoted by the superscript "L", and the liquid film adjacent to the solid catalyst phase will be denoted by a superscript "S". To model mass transfer in these films, the Maxwell−Stefan equations are used. Thermodynamic equilibrium is assumed only at the vapor/liquid interface. Mass transfer inside the porous catalyst will be described with the so-called dusty fluid model, discussed in a later section. We assume the reaction takes place only in the catalyst phase. Thus, the chemical reaction term disappears from the liquid-phase balances. We also need to add a term for mass transfer from the bulk liquid to the catalyst phase and the liquid-phase mass balance becomes

$$L_k - L_{k-1} - N^{\mathrm{L}}_{t,k} - N^{\mathrm{S}}_{t,k} = 0 \tag{1}$$

There are no changes in the vapor-phase mass balance:

$$V_k - V_{k+1} + N^{\mathrm{V}}_{t,k} = 0 \tag{2}$$

Here, L_k is the liquid molar flow from cell k and V_k is the vapor flow rate from stage k. $N^{\mathrm{L}}_{t,k}$ and $N^{\mathrm{V}}_{t,k}$ are the liquid and vapor interphase mass-transfer rates. $N^{\mathrm{S}}_{t,k}$ is the overall mass-transfer rate in the liquid film around the catalyst. For an equistoichiometric reaction $N^{\mathrm{S}}_{t,k}$ is zero. A term for the species fluxes appears in the individual component balance for the liquid phase:

$$L_k x_{i,k} - L_{k-1} x_{i,k-1} - N^{\mathrm{L}}_{i,k} - N^{\mathrm{S}}_{i,k} = 0 \tag{3}$$

The vapor-phase mass balance for the nonequilibrium cell remains unchanged:

$$V_k y_{i,k} - V_{k+1} y_{i,k+1} + N^{\mathrm{V}}_{i,k} = 0 \tag{4}$$

$y_{i,k}$ and $x_{i,k}$ are the vapor and liquid mole fractions of component i in cell k. $N^{\mathrm{V}}_{i,k}$ and $N^{\mathrm{L}}_{i,k}$ are the individual component mass-transfer rates of component i in the transfer films at the vapor/liquid interface and $N^{\mathrm{S}}_{i,k}$ is the individual component mass-transfer rate of component i in the transfer film around the catalyst; the latter will only be zero if component i is not a reactant. The liquid- and vapor-phase energy balances are not changed:

$$L_k H^{\mathrm{L}}_k - L_{k-1} H^{\mathrm{L}}_{k-1} - \epsilon^{\mathrm{L}}_k = 0 \tag{5}$$

$$V_k H^{\mathrm{V}}_k - V_{k+1} H^{\mathrm{V}}_{k+1} + \epsilon^{\mathrm{V}}_k = 0 \tag{6}$$

H^{L} and H^{V} are the liquid and vapor enthalpies and ϵ^{L} and ϵ^{V} are the liquid and vapor interphase energy-transfer rates. Note that there is no entry for an energy-transfer rate to the catalyst. This is due to the fact that at steady state the energy transfer to the catalyst is zero; otherwise, we would have accumulation of energy inside the catalyst.

The mass-transfer rates between the vapor and liquid phases are calculated using the Maxwell−Stefan equations.[23] The mass-transfer rates through the interface have to be continuous:

$$N^{\mathrm{L}}_{i,k} = N^{\mathrm{V}}_{i,k} \tag{7}$$

The same is true for the energy-transfer rates:

$$\epsilon^{\mathrm{L}}_k = \epsilon^{\mathrm{V}}_k \tag{8}$$

This last equation plays a very important role in determining the actual mass-transfer rates. The Maxwell−Stefan equations by themselves are "floating equations". They relate the driving force for mass transfer of a component to the friction of the other species on that component. This is done in terms of relative component velocities. These relative velocities are "tied down" by eq 8, which is commonly referred to as the "bootstrap" relation.[23,27]

For more details about the incorporation of the Maxwell−Stefan equations into the nonequilibrium cell model, see Higler et al.[20]

The Maxwell-Stefan equations are also used for description of mass transport in the liquid−solid mass-transfer film. The cell indices have been dropped for clarity.

$$\frac{x_i}{R\,T}\frac{\partial \mu^{\mathrm{L}}_i}{\partial \eta} = \sum_{l=1}^{c} \frac{x_i N^{\mathrm{S}}_l - x_l N^{\mathrm{S}}_i}{c^{\mathrm{L}}_{\mathrm{t}}(\kappa^{\mathrm{L}}_{i,l} a^{\mathrm{C}})} \tag{9}$$

The mass-transfer coefficient, $\kappa^{\mathrm{L}}_{i,l}$, has to be calculated from an appropriate correlation for liquid/solid mass transfer. Only $c - 1$ of these equations are independent. The mole fraction of the cth component follows from the summation equation:

$$\sum_{i=1}^{c} x_i = 1 \tag{10}$$

In addition, the energy flux through the liquid film around the catalyst is zero:

$$\epsilon_j^{\mathrm{L}} = -h^{\mathrm{L}} a^{\mathrm{C}} \frac{\partial T}{\partial \eta} + \sum_{i=1}^{c} N_i^{\mathrm{L}} H_i^{\mathrm{L}} = 0 \tag{11}$$

The major new problem we have to deal with in this nonequilibrium model involves liquid-phase multicomponent mass transfer with reaction in the porous catalyst. For this, there is, however, no complete theory. Even for gases, for which there is a kinetic theory, there are complete and internally consistent theories of multicomponent mass transfer in porous media only for two cases. When the pore size is much smaller than the mean free path length, there is the Knudsen diffusion theory, and the kinetic theory applies when the pore size is orders of magnitudes longer than the mean free path length. However, for the intermediate regime there are substantial problems. The molecular velocity distribution varies in a complicated way over the cross section of the pore and additional problems are posed by catalyst geometry and pore size distribution.

We will, therefore, first describe the theory of gas-phase multicomponent mass transfer in porous media and subsequently discuss a modification of these equations suitable for liquid-phase systems.

2.1. Dusty Gas Model. Modeling multicomponent mass transfer in porous media is complicated when the mean free path length of the molecules is of the order of magnitude of the pore diameter. The difficulties posed by this intermediate case may be circumvented by a method originally introduced by Maxwell[28] and developed further by Mason and various co-workers.[29−33] The original idea of Maxwell is as follows: "We may suppose the action of the porous material to be similar to that of a number of particles, fixed in space and obstructing the motion of the particles of the moving systems."

In other words, he suggested that the porous material itself be described as a supplementary "dust" species, consisting of very large molecules that are kept motionless by some unspecified external force. The Chapman−Enskog kinetic theory is then applied to the new pseudo gas mixture, whereby the interaction between the dust and gas molecules simulates the interaction between the solid matrix and the gas species. In addition, one is no longer faced with the problem of flux and composition variations across a pore and problems related to catalyst geometry.

The price we have to pay for this simplification is that we "lose" certain physical features of the porous medium. One of the more important issues is that we are no longer dealing with channels of finite size corresponding to the pores in the real medium. Thus, there is no introduction of the viscous fluxes in the formal development of the equations. These have to be added empirically, although Mason et al. presented arguments to justify the addition of diffusive and viscous fluxes. In what follows, we will first derive the diffusive part of the equations and subsequently deal with the viscous fluxes.

For diffusion of an ideal gas mixture in "open space" the "generalized Maxwell−Stefan equations" (GMS) are[34]

$$d_i \equiv \frac{x_i}{RT}(\nabla \mu_i)_{T,p} + \frac{\phi_i - \omega_i}{c_t RT}\nabla p - \frac{1}{c_t RT}(c_i F_i - \omega_i \sum_{j=1}^{c} c_j F_j) + \sum_{j=1}^{c} x_i x_j \alpha_{i,j} \nabla(\ln(T)) = \sum_{j=1}^{c} \frac{x_i N_j - x_j N_i}{c_t \mathrm{Đ}_{i,j}} \tag{12}$$

The left-hand side of this equation represents the sum of the driving forces. The first term represents the driving force due to a chemical potential gradient $\nabla\mu_i$. The second term represents a driving force due to a pressure gradient ∇p. This term will be important only if the volume fraction ϕ_i and mass fraction ω_i of component i are not the same. The third term is the driving force for forced diffusion. This may be the case for charged particles in an electric field. The last term represents thermal diffusion. In most cases encountered in distillation, extraction, or gas absorption, the thermal diffusion term is very much smaller than the other terms and may safely be neglected. The right-hand side of the equation represents the sum of the molecular friction terms.

For an ideal gas the chemical potential gradient term simplifies as follows:

$$\frac{x_i}{RT}(\nabla \mu_i)_{T,p} = \nabla x_i \tag{13}$$

In addition, the volume fraction and mole fractions will be the same for each component:

$$\phi_i = x_i \tag{14}$$

Furthermore, the concentration of the mixture may be expressed in terms of pressure and temperature by means of the ideal gas law:

$$c_t = \frac{p}{RT} \tag{15}$$

To obtain the dusty gas model equations, eq 12 is applied to a pseudo mixture of $c + 1$ species in which the extra species represents the catalyst phase. The dust species is subject to the following constraints:

1. The dust must be equally distributed in space: $\nabla c_{c+1} = 0$.
2. The dust is kept immobile by an unspecified external force so that $N_{c+1} = 0$.
3. The dust species consists of giant molecules whose molar mass goes to infinity: $M_{c+1} \rightarrow \infty$.

The unspecified forces in item 2 prevent the porous medium from moving because of pressure gradients in the gas. This will be the force exerted by the catalyst matrix to keep everything in place. Furthermore, for the cases considered in this paper, there are no external forces on the gaseous species, so that $F_l = 0$ for l from 1 to c.

When eq 12 is applied to the pseudo mixture of $c + 1$ components, variables such as mole fractions and concentrations will be those of the pseudo mixture, including the dust molecules. In the subsequent derivation of the dusty gas model equations these variables will be marked by a tilde to distinguish them from the true quantities in the mixture. For the species concen-

trations, partial pressures and component fluxes, there is no difference between the pseudo quantities and the real quantities.

Applying eq 12 to the pseudo mixture, under the above assumptions, lead to

$$d_i \equiv \nabla\tilde{x}_i + \frac{\tilde{x}_i - \tilde{\omega}_i}{\tilde{p}}\nabla\tilde{p} + \frac{\tilde{\omega}_i}{\tilde{p}}\, c_{c+1}F_{c+1} = \sum_{l=1}^{c}\frac{\tilde{x}_i N_l - \tilde{x}_l N_i}{\tilde{c}_t\tilde{\mathfrak{D}}_{i,l}} - \frac{\tilde{x}_{c+1}}{\tilde{c}_t\tilde{\mathfrak{D}}_{i,c+1}N_i} \tag{16}$$

From hydrodynamic considerations it follows that the force exerted by the gas on the porous medium is equal to the physical pressure gradient of the gas over the porous medium:

$$c_{c+1}F_{c+1} = \nabla p \tag{17}$$

We need only relate the variables pertaining to the pseudo mixture to those of the real gas. The complete derivation is given by Jackson.[34] The result is eq 18:

$$\frac{1}{RT}\nabla p_i = \sum_{j=1}^{c}\frac{x_i N_j^{\mathrm{D}} - x_j N_i^{\mathrm{D}}}{\mathfrak{D}_{i,j}^{\mathrm{e}}} - \frac{N_i^{\mathrm{D}}}{D_i^{\mathrm{e}}} \tag{18}$$

The "D" has been added as superscripts to emphasize that these variables are the *diffusive* flux relations associated with the dusty gas model. We also have viscous fluxes that arise from movement of the mixture as a whole. This is related to the flow of a pure substance in a cylindrical tube and is described by the standard Poiseuille flow problem. For a circular tube of diameter d_p, the contribution to the molar flux due to viscous flow is

$$N^{\mathrm{V}} = -\frac{{d_p}^2 p}{32\eta RT}\frac{\mathrm{d}p}{\mathrm{d}z} \tag{19}$$

For a porous medium with a distribution of pore sizes, we may rewrite this equation as[34]

$$N^{\mathrm{V}} = -\frac{B_0 p}{\eta RT}\frac{\mathrm{d}p}{\mathrm{d}z} \tag{20}$$

This equation defines the permeability B_0. When all the pore sizes are uniform and of diameter d_p, the permeability is given by

$$B_0 = \frac{{d_p}^2}{32} \tag{21}$$

If we are dealing with a gas mixture instead of a pure gas, and there is no diffusion of the species in the mixture relative to the mixture as a whole, then the total viscous flux for component i (in all directions) is given by

$$N_i^{\mathrm{V}} = -\frac{x_i B_0 p}{\eta RT}\nabla p \tag{22}$$

The flux of component i is given by adding the diffusive and convective fluxes:

$$N_i = N_i^{\mathrm{D}} + N_i^{\mathrm{V}} \tag{23}$$

Equations 18, 22, and 23 may now be combined to give the complete dusty gas model equations:

$$\frac{1}{RT}\nabla p_i + \frac{x_i B_0 p}{\eta RT D_i^{\mathrm{e}}}\nabla p = \sum_{j=1}^{c}\frac{x_i N_j - x_j N_i}{\mathfrak{D}_{i,j}^{\mathrm{e}}} - \frac{N_i}{D_i^{\mathrm{e}}} \tag{24}$$

Rearranging once more gives the working form of the dusty gas model equations:

$$\frac{p}{RT}\nabla x_i + \frac{x_i}{RT}\left(1 + \frac{B_0 p}{\eta D_i^{\mathrm{e}}}\right)\nabla p = \sum_{j=1}^{c}\frac{x_i N_j - x_j N_i}{\mathfrak{D}_{i,j}^{\mathrm{e}}} - \frac{N_i}{D_i^{\mathrm{e}}} \tag{25}$$

2.2. Dusty Fluid Model. The "dusty fluid model" as developed by Krishna and Wesselingh[27] is a modification of the "dusty gas model" so as to be able to model liquid-phase diffusion in porous media. First, all pressure terms are replaced with concentrations by back-substituting the ideal gas law ($p = c_t RT$). Note that this was done for convenience in the derivation of the "dusty gas equations". Equation 25 may be rewritten as

$$\nabla x_i + \frac{x_i}{p}\nabla p + \frac{x_i B_0}{\eta D_i^{\mathrm{e}}}\nabla p = \sum_{j=1}^{c}\frac{x_i N_j - x_j N_i}{c_t\mathfrak{D}_{i,j}^{\mathrm{e}}} - \frac{N_i}{c_t D_i^{\mathrm{e}}} \tag{26}$$

The first two terms in this equation correspond to the isothermal chemical potential gradient for an ideal mixture, which may be split up as follows:

$$\nabla x_i + \frac{x_i}{p}\nabla p = \nabla_T \mu_i = \nabla_{T,p}\mu_i + \bar{V}_i\nabla p \tag{27}$$

For a nonideal mixture we have

$$\frac{x_i}{RT}\nabla_{T,p}\mu_i + \frac{x_i}{RT}\bar{V}_i\nabla p + \frac{x_i B_0}{\eta D_i^{\mathrm{e}}}\nabla p = \sum_{j=1}^{c}\frac{x_i N_j - x_j N_i}{c_t\mathfrak{D}_{i,j}^{\mathrm{e}}} - \frac{N_i}{c_t D_i^{\mathrm{e}}} \tag{28}$$

Equation 28 is expressed in terms of diffusion coefficients and fluxes, rather than mass-transfer coefficients and mass-transfer rates as is done for the liquid and vapor film transfer equations. The mass-transfer rates are obtained by multiplying the fluxes by the interfacial area of the catalyst particles. This is not as straightforward, as it looks, since depending on the geometry of the catalyst, the cross-sectional area can change along the diffusion path. In addition, one should take the different geometries into account in the derivation of the discretized equations. This will be discussed in detail below.

The dusty fluid model equations do not sum up to zero (unlike the GMS equations) because of the pressure term, leading to an extra equation for the pressure drop. Summing up over the c species gives

$$\sum_{i=1}^{c}\frac{N_i}{D_i^{\mathrm{e}}} = -\frac{1}{RT}\left(1 + \frac{c_t B_0 RT}{\eta}\sum_{i=1}^{c}\frac{x_i}{D_i^{\mathrm{e}}}\right)\nabla p \tag{29}$$

because

$$\sum_{i=1}^{c}\sum_{j=1}^{c}\frac{x_j N_i - x_i N_j}{Đ_{i,j}^{e}} = 0 \tag{30}$$

and the Gibbs−Duhem equation:

$$\sum_{i=1}^{c}\frac{c_i}{R\ T}\nabla_{T,p}\mu_i = 0 \tag{31}$$

Not all of the above equations are independent. We can choose either c times eq 28 while discarding eq 29 or $c - 1$ times eq 28 together with eq 29.

Because there can be no accumulation of mass in the catalyst particle at steady state, the following equation has to be satisfied:

$$\sum_{i=1}^{c} M_i N_i = 0 \tag{32}$$

This equation provides the "bootstrap" condition for the dusty fluid equations.

The component fluxes will change due to reaction

$$\frac{\partial N_i}{\partial z} = \sum_{i=1}^{c}\nu_{i,m}R_m \tag{33}$$

The total energy flux in a catalyst particle is zero because at steady state there can be no accumulation inside the catalyst. Therefore,

$$\epsilon^{C} = q + \sum_{i=1}^{c} H_i^{L} N_i = 0 \tag{34}$$

2.3. Boundary Conditions. The boundary conditions at the outer surface of the catalyst are provided by the mass balances around the catalyst particle. In addition, the mass-transfer rates at the catalyst interface should be continuous:

$$N_{i,j}^{S} = N_{i,j}^{C} \tag{35}$$

At the catalyst center, the temperature, pressure, and composition have zero gradients:

$$\frac{\partial p}{\partial \eta} = 0; \quad \frac{\partial T}{\partial \eta} = 0; \quad \frac{\partial x_i}{\partial \eta} = 0 \tag{36}$$

And the flux of species i is zero:

$$N_i = 0 \tag{37}$$

This concludes the development of the dusty fluid model for mass transfer in porous media.

2.4. Discretization and Geometry. When the dusty fluid equations are discretized, the catalyst shape plays an important role. For Raschig ring type packings, it is possible to use a simple Cartesian coordinate system. However, this approach is not recommended for teabag- and sandwich-type packings, where smaller catalyst particles can be used. First, however, the multidimensional problem is simplified by replacing the gradient terms by derivatives with respect to one direction coordinate. In addition, because we prefer to deal with mass-transfer rates, the fluxes are multiplied by the interfacial area. Equation 28 becomes

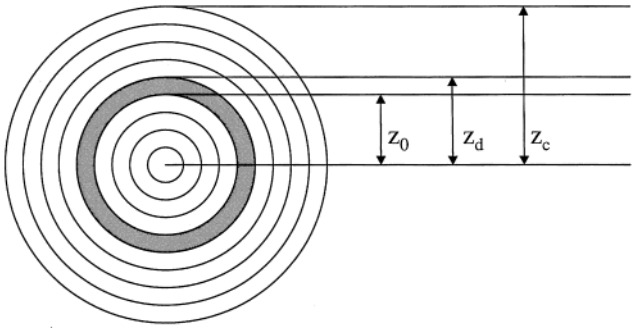

Figure 2. Schematic representation of the grid for a catalyst particle.

$$\frac{x_i}{R\ T}\frac{\partial \mu_i}{\partial z} + x_i\left(\frac{\bar{V}_i}{R\ T} + \frac{B_0}{\eta D_i^{e}}\right)\frac{\partial p}{\partial z} = \sum_{l=1}^{c}\frac{x_i N_l - x_l N_i}{c_t Đ_{i,l}^{e} a^{C}} - \frac{N_i}{c_t D_i^{e} a^{C}} \tag{38}$$

Assuming that we are dealing with a catalyst particle with radius z_c, this particle will be split up in a number of finite volumes, as illustrated in Figure 2. Subsequently, the dusty fluid model equations are applied to each finite volume individually. This has some consequences for the differential terms and interfacial areas in the above equation. For the differential term of an arbitrary quantity X,

$$\frac{\partial X}{\partial z} = \frac{1}{L}\frac{\partial X}{\partial \eta} = \frac{X_k - X_{k-1}}{L} \tag{39}$$

where L is a characteristic length for diffusion in the film under consideration.[23]

For a planar film,

$$L = z_d - z_0$$

For a cylindrical film,

$$L = r_0 \ln(z_d/z_0)$$

For a spherical film,

$$L = z_0(1 - z_d/z_0)$$

The cross-sectional area for cylindrical and spherical catalysts depends on the location in the film as well. This can be accounted for by relating the area ratio of the catalyst area at location k to the outside catalyst area. For the various geometries this ratio can be represented by

$$r_a = \left(\frac{z_d}{z_c}\right)^{\alpha} \tag{40}$$

whereby $\alpha = 0$ for a planar film, 1 for a cylindrical film, and 2 for a spherical film.

The chemical potential gradient is approximated as

$$\left(\frac{x_i}{R\ T}\frac{\partial \mu_i}{\partial \eta}\right)_k = \sum_{l=1}^{c-1}(\Gamma_{i,j})_k\frac{(x_i)_k - (x_i)_{k-1}}{L} \tag{41}$$

in which

$$\Gamma_{i,j} = \delta_{i,j} + x_i\left(\frac{\partial \ln(\gamma_i)}{\partial x_j}\right)_{T,P,x_k,k\neq j=1\ldots c-1} \quad (42)$$

The central difference scheme will not be used here because this has the tendency to generate zigzag profiles. Using the above discretization scheme does not give these problems but does introduce a numerical diffusion term. A sufficiently large number of discretization points must be used to minimize the effect of this term. For the pressure and temperature derivatives central difference approximations will be used. Note that, depending on the geometry, the discretization step length varies per discretization point. Taking everything into account, the discretized dusty fluid equations become

$$\sum_{l=1}^{c-1}(\Gamma_{i,j})_k\frac{(x_i)_k - (x_i)_{k-1}}{L} + (x_i)_k\left(\frac{\bar{V}_i}{R\ T} + \frac{B_0}{\eta D_i^e}\right)\left(\frac{p_{k+1} - p_k}{2L_{\ k}} + \frac{p_k - p_{k-1}}{2L_{\ k-1}}\right) = \sum_{l=1}^{c}\frac{(x_i)_k N_l - (x_l)_k N_i}{c_t \mathcal{D}_{i,l}^e a^C r_a} - \frac{N_{\ i}}{c_t D_i^e a^C r_a} \quad (43)$$

The catalyst shape also influences the reaction equation. In effect, eq 33 is a conservation equation, the expressions for the different catalyst shapes may be derived by writing a mass balance for a finite volume of the catalyst,

$$(N_i a)_k - (N_i a)_{k+1} = \sum_{m=1}^{nr}\nu_{i,m}R_m\epsilon_k V_c \quad (44)$$

where V_c is the total catalyst volume available in the contacting cell and ϵ_k is the volume fraction of the slice of catalyst (see Figure 2) under consideration.

The fluxes may be replaced by mass-transfer rates, taking into account the interfacial area ratio. The volume fraction of the catalyst is obtained by taking the volume fraction under consideration and divide by the total catalyst volume. A general expression for the volume fraction is given by

$$\epsilon_k = \frac{r_\delta^\beta - r_0^\beta}{r_c^\beta} \quad (45)$$

where $\beta = 1$ for a planar catalyst, $\beta = 2$ for a cylindrical catalyst, and $\beta = 3$ for a spherical catalyst. The resulting discretized conservation equation then becomes

$$(N_{\ i}^C r_a)_k - (N_{\ i}^C r_a)_{k+1} = \sum_{m=1}^{nr}\nu_{i,m}R_m\epsilon_k V_c \quad (46)$$

The last equation to be discretized is the energy-transfer equation. The energy-transfer rate equation consists of a convective and a conductive contribution. We shall assume that the catalyst matrix and the liquid filling the pores have the same temperature profile. The total conductive energy flux may then be written as

$$q = -\left((1-\epsilon)\lambda^C + \lambda^L\frac{\epsilon}{\tau}\right)\nabla T \quad (47)$$

Table 1. Variables Related to the Dusty Fluid Model

For the Bulk of Each Cell		
catalyst mass-transfer rates	$N_{i,k}^S$	c
For Liquid Film S, n_3 Discretization Points		
composition	$x_{i,k}$	cn_3
temperatures	T_k	n_3
Inside the Catalyst, n_4 Discretization Points		
composition	$x_{i,k}$	cn_4
temperatures	T_k	n_4
catalyst mass-transfer rates	$N_{i,k}^C$	cn_4
catalyst pressure	p	n_4

Table 2. Equations Related to the Dusty Fluid Model

For Liquid Film S, n_3 Discretization Points		
Maxwell−Stefan equations	eq 9	$(c-1)n_3$
summation equation	eq 10	n_3
energy-transfer equation	eq 11	n_3
For the Catalyst n_4 Discretization Points		
dusty fluid equations	eq 28	$c(n_4-1)$
summation equation	eq 10	n_4-1
reaction equation	eq 33	$n_4(c-1)$
"bootstrap" equation	eq 32	n_4
energy-transfer equation	eq 34	n_4-1
boundary conditions	eqs 36 and 37	$2c+2$

The catalyst porosity and tortuosity are added here to take into account the curved paths followed by the gas in the catalyst. The discretized equation is then given by

$$q = -\left((1-\epsilon)\lambda^C + \lambda^L\frac{\epsilon}{\tau}\right)\left(\frac{T_{k+1} - T_k}{2L_{\ k}} + \frac{T_k - T_{k-1}}{2L_{\ k-1}}\right) \quad (48)$$

Combining the convective and conductive contributions and multiplying by the interfacial area then gives

$$-a^C(r_a)_k\left((1-\epsilon)\lambda^C + \lambda^L\frac{\epsilon}{\tau}\right)\left(\frac{T_{k+1} - T_k}{2L_{\ k}} + \frac{T_k - T_{k-1}}{2L_{\ k-1}}\right) + \sum_{i=1}^{c}N_{\ i}^C H_{\ i} = 0 \quad (49)$$

3. Model System

A complete degree of freedom analysis for the nonequilibrium cell model is given by Higler et al.[20] Here, only the additional variables and equations important for the dusty gas model are discussed. The variables are listed in Table 1. n_3 is the number of discretization points in the liquid film around the catalyst and n_4 is the number of discretization points inside the catalyst. The total number of variables related to the dusty fluid model equations is $(c + (c+1)n_3 + (2c+2)n_4)$. The equations required for the dusty fluid model are given in Table 2. For each cell, the number of equations is $(c + (c+1)n_3 + (2c+2)n_4)$, which is the same as the number of variables. There are, therefore, no degrees of freedom in the dusty fluid model equations.

For a system of c components, a column of n_s nonequilibrium stages, a reboiler and a condensor, n_c cells per nonequilibrium stage, using n_1 discretization points in the liquid film, and n_2 discretization points in the vapor film, using the above catalyst layout, the total number of independent equations for this nonequilibrium cell model is $n_s(2c + 5 + n_c(7c + 5 + n_1(2c+1) + n_2(c+1) + (c+1)n_3 + (2c+2)n_4) + 4c + 8$. The total number of variables is just two more than this. Thus, the number of degrees of freedom is 2. Possible specifications for this model are discussed by Higler et al.[20]

The model requires data about the actual design. This link between model and design has been discussed extensively by Taylor et al.,[35] who proposed an integration of a column design procedure with the model equations. During the calculations, a column design is designed based on the calculated liquid and vapor flows and physical properties. For more details, see Taylor et al.[35] and Kooijman.[36] At the very least, one is required to specify only an internals type, although specification of detailed designs also is a possibility.

4. Physical Properties

In the dusty fluid model there are several parameters that need to be known so that a simulation can be carried out.

4.1. Catalyst Properties. The following catalyst data need to be known beforehand:

(1) specific catalyst area, a^C;
(2) catalyst porosity, ϵ^C;
(3) catalyst tortuosity, τ^C;
(4) catalyst mean pore size, d_p;
(5) catalyst thermal conductivity, λ^C.

The porosity and tortuosity are required for evaluation of the catalyst diffusion coefficients. The mean pore size is required for evaluation of the catalyst permeability. The catalyst thermal conductivity is required for calculation of the conductive contribution of the catalyst matrix to heat transfer inside the catalyst particles.

4.2. Thermodynamic Parameters. Inside the catalyst, nonideal component behavior will be influenced by the catalyst itself. For a consistent description one should incorporate the effect of the catalyst into evaluation of the chemical potential gradients. No suitable model for this is available. For evaluation of the chemical potential gradients a conventional activity coefficient model will be used.

4.3. Mass-Transfer Parameters. Estimation of the mass-transfer coefficients and of the physical properties for the vapor/liquid transport process is discussed at length by Taylor and Krishna.[23] For mass transfer from the liquid bulk to the catalyst phase the correlations due to van Krevelen and Krekels[37] were used. These are

$$\frac{\kappa_{i,j}^{LS}}{Đ_{i,j}^{L} a^{C}} = 1.8\left(\frac{\rho^{L} u^{L}}{\eta^{L} a^{C}}\right)^{1/2}\left(\frac{\eta^{L}}{\rho^{L} Đ_{i,j}^{L}}\right)^{1/3} \tag{50}$$

Under the condition that

$$0.013 < \frac{\rho^{L} u^{L}}{\eta^{L} a^{C}} < 12.6 \tag{51}$$

The binary pair Maxwell−Stefan diffusion coefficients ($Đ_{i,j}^{e}$) are related to the free diffusion binary pair Maxwell−Stefan diffusion coefficients by

$$Đ_{i,j}^{e} = \frac{\epsilon}{\tau} Đ_{i,j} \tag{52}$$

where ϵ is the catalyst porosity and τ is the catalyst tortuosity. The catalyst porosity and tortuosity are added here to take into account the tortuous paths followed by the fluid in the catalyst.

Consider the case of very large pores where the effects of the walls will be negligible. This assumption is valid for the macroporous catalysts used by Sundmacher et al.,[4] as it will be in most cases. In this case, one could argue that we are basically dealing with a simple free diffusion problem. The diffusion coefficients would be the normal liquid-phase Maxwell−Stefan diffusion coefficients, corrected by the catalyst tortuosity and porosity as in eq 52. Berg and Harris[38] and Sundmacher and Hoffmann[25] have used this approach but these authors have ignored the last term on the right-hand side of eq 28. There is no available theory for the estimation of D_i^e for liquid diffusion inside porous particles. In the calculations presented later in this paper we consider two limiting cases: (a) one in which D_i^e is large, in which case the last term can be ignored (corresponding to Berg−Harris and Sundmacher approaches), and (b) one in which D_i^e is a factor 5 times smaller than the smallest of the $Đ_{i,j}$ values. D_i^e is assumed to be the same for all components.

Diffusion coefficients normally are concentration dependent. Thus, they should be dependent on the concentration and the physical properties of the dust species. Any such dependence is, however, neglected here because of the absence of any reliable estimation method.

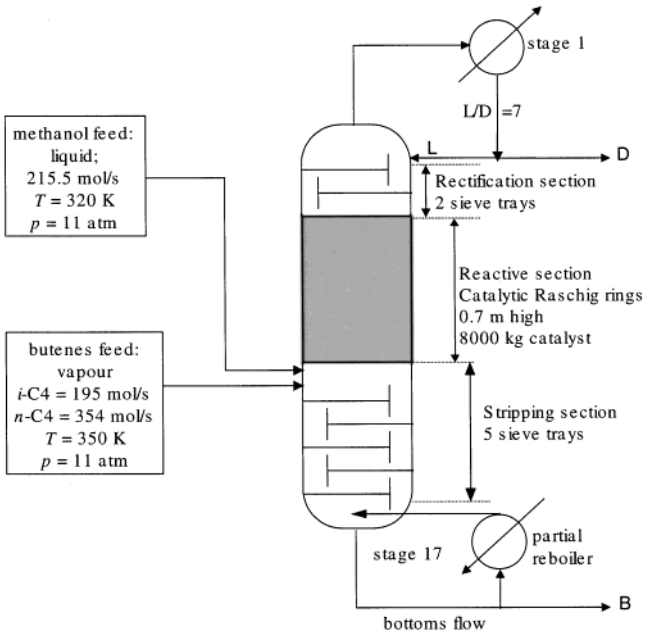

Figure 3. Schematic representation of a reactive distillation column for MTBE production.

5. Results and Discussion

5.1. MTBE Case Study. Our first case study involves the reactive distillation process shown in Figure 3 and is based on an example in Jacobs and Krishna.[39] For details about column internals see Higler et al.[21] Higler et al.[21] have shown that there can be substantial differences between the results of equilibrium and nonequilibrium models for this process. In addition, it was shown that even minor changes in the magnitude of the mass-transfer coefficients can have a substantial influence on the location of the multiple steady-state region. Furthermore, Baur et al.[40] show that there are substantial differences between a full Maxwell−Stefan description and an equal diffusivity model of mass transfer. Both of those studies used a pseudohomogeneous model for the reaction.

Table 3. Base Values and Tested Ranges for Model Parameters

parameter	base value	range considered
catalyst thickness, m	0.5×10^{-3}	0.25×10^{-3} to 1.0×10^{-3}
catalyst porosity	0.6	0.5−0.7
catalyst tortuosity	1.5	1−2
catalyst thermal conductivity, $J \cdot K^{-1} \cdot m^{-1} \cdot s^{-1}$	λ^L	$0.01\lambda^L - 100\lambda^L$

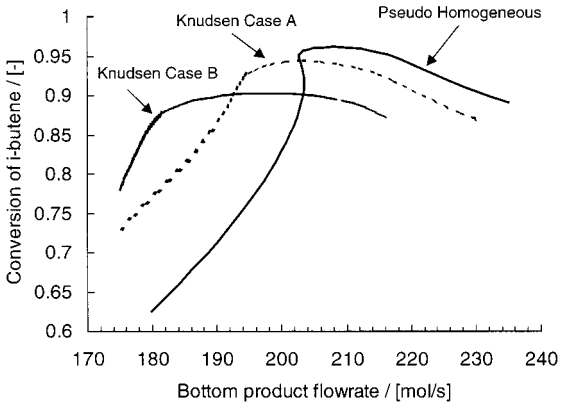

Figure 4. Steady-state conversion of isobutene in a MTBE column as a function of the bottom product flow rate. Comparison of pseudohomogeneous and dusty fluid models.

In this work we have used the dusty fluid model and repeated the calculations described by Higler et al.[39] and Baur et al.[40] The catalyst shape was assumed to be planar. This may be a reasonable approximation for Raschig rings, if they are not too thick. The outside catalyst area was set to 600 m^2/m^3.[26] Other property values are summarized in Table 3.

Figure 4 shows the steady-state conversion of isobutene as a function of the bottom product flow rate for the pseudohomogeneous model and for the dusty fluid model. Knudsen case A corresponds to a situation in which the Knudsen diffusion coefficient in the dusty fluid model is taken to be 2 orders of magnitude larger than the average binary pair diffusion coefficient. Knudsen case B represents the case for which the Knudsen diffusion coefficient was taken to be one-fifth of the lowest binary pair diffusion coefficient of the mixture.

Two observations can be made immediately: First, the multiple steady-state region has completely disappeared for the dusty fluid model, and second, the Knudsen diffusion term has a substantial influence on the results of the dusty fluid model simulations.

The first observation can be explained by the fact that in the lower branch of the multiple steady-state region in part of the reactive section the reverse reaction (reaction of MTBE to methanol and isobutene) takes place. Introduction of a mass-transfer resistance to account for transport inside the catalyst reduces the influence of this backward reaction. The introduction of extra mass-transfer resistances also leads to the observed drop in the maximum achievable conversion. Furthermore, Knudsen case B includes an additional resistance term due to Knudsen diffusion. Thus, the model predicts an even lower maximum conversion than that for Knudsen case A. One conclusion that can be drawn from these findings is that equilibrium models tend to exaggerate the phenomenon of multiple steady states and the addition of mass-transfer resistances

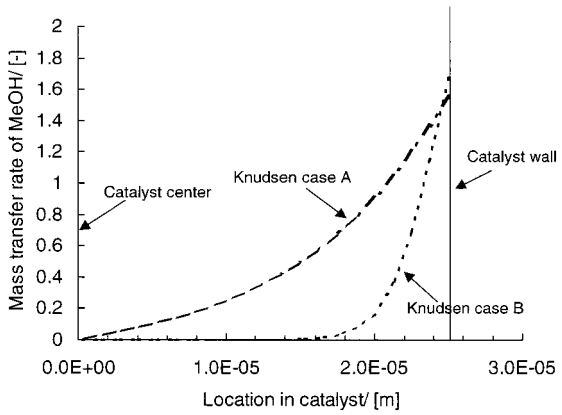

Figure 5. Mass-transfer rates inside catalyst particles.

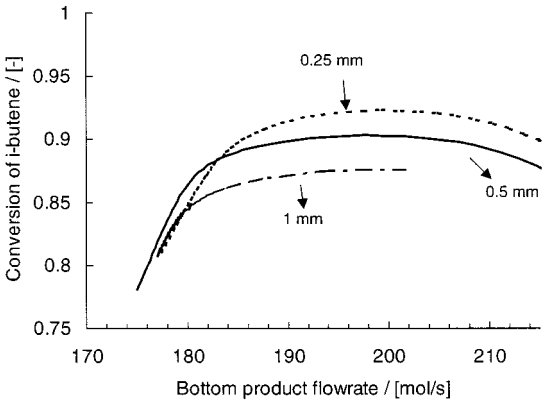

Figure 6. Conversion of isobutene as a function of the bottom product flow rate for various catalyst thicknesses.

results in a much smaller realizable "window" for the multiple steady states.

Figure 5 shows the mass-transfer rates in the catalyst on stage 15 obtained with the dusty fluid model for both Knudsen cases at a bottom product flow rate of 200 mol/s. The situation shown in Figure 5 is representative for all stages. In Knudsen case B, mass transfer inside the catalyst only takes place in a small section close to the catalyst outside surface (catalyst wall). For Knusden case A, mass transfer takes place throughout the entire catalyst particle. Because changes in the mass-transfer rate correspond to the rate of reaction (see eq 33), it follows that in Knudsen case B only part of the catalyst is used for chemical conversion.

The values of the catalyst thickness, catalyst porosity, and other parameters were all varied over the ranges given in Table 3.

For Knudsen case A we found no significantly different results for any of these parameter variations. For Knudsen case B, the influence of the catalyst thickness is substantial. Shown in Figure 6 is the steady-state conversion of isobutene as a function of the bottom product flow rate for various catalyst thicknessess. The maximum achievable conversion is significantly lower for the thicker catalyst. This is due to the fact that, for Knudsen case B, the column operates in a diffusion-limited regime.

Additional calculations were done in which the mass-transfer resistances to and inside the catalyst were neglected. This can be done by multiplying the outside catalyst area by a very large number. These calculations confirm our expectation that with removal of these additional mass-transfer resistances the full nonequi-

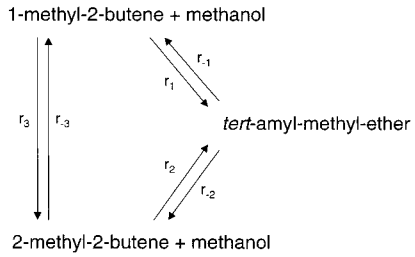

Figure 7. Schematic representation of the reaction system.

librium dusty fluid model gave results that were the same as those obtained with the pseudohomogeneous model.

5.2. TAME Case Study. For our second case study we will consider the reactive distillation process for *tert*-amyl methyl ether (TAME). The reaction under consideration is the acid-catalyzed formation of TAME from 2-methyl-1-butene, 2-methyl-2-butene, and methanol using a heterogeneous catalyst. Extensive discussions on the kinetics of the above reaction is given by Oost and Hoffmann[41] and Rihko and Krause.[42] The reaction system is depicted schematically in Figure 7.

TAME is formed out of the two pentene isomers, for which we can write the following reaction equations:

$$r_1 = k_1\left(\frac{a_{2M1B}}{a_{MeOH}} - \frac{1}{K_1}\frac{a_{TAME}}{a_{MeOH}^2}\right) \tag{53}$$

$$r_2 = k_2\left(\frac{a_{2M2B}}{a_{MeOH}} - \frac{1}{K_2}\frac{a_{TAME}}{a_{MeOH}^2}\right) \tag{54}$$

In addition, there is a rapid isomerization reaction between the two pentene isomers:

$$r_3 = k_3\left(a_{2M1B} - \frac{1}{K_3}a_{2M2B}\right) \tag{55}$$

The equilibrium constants for the above reactions are given by Rihko et al. (1994):

$$K_1 = 1.057 \times 10^{-4} \exp\left\{\frac{4273.5}{T}\right\} \tag{56}$$

$$K_2 = 1.629 \times 10^{-4} \exp\left\{\frac{3374.4}{T}\right\} \tag{57}$$

$$K_3 = \frac{K_1}{K_2} = 0.648 \exp\left\{\frac{899.1}{T}\right\} \tag{58}$$

Because of the rapid isomerization reaction, it is very hard to determine the individual rate constants of the first two reactions separately. Therefore, lumped reaction kinetics has to be used. The overall reaction rate of TAME is given by summation and rearrangement of eqs 53 and 54:

$$r_{1+2} = (k_1 + k_2K_3)\left(\frac{a_{2M1B}}{a_{MeOH}} - \frac{1}{K_1}\frac{a_{TAME}}{a_{MeOH}^2}\right) \tag{59}$$

Thiel et al.[43] give the following expression for the forward reaction rate constant:

$$k_1 + k_2K_3 = (1 + K_3) \times 2.576 \exp\left\{32.3 - \frac{10764}{T}\right\} \tag{60}$$

Table 4. Wilson Parameters for TAME System

component *i*	component *j*	$a_{i,j}$, J/mol	$a_{j,i}$, J/mol
methanol	2-methyl-1-butene	9772.3	1376.5
methanol	2-methyl-2-butene	10 147	968.81
methanol	methyl *tert*-pentyl ether	4826.3	−177
methanol	*n*-pentane	11 749	1946.7
2-methyl-1-butene	methyl *tert*-pentyl ether	487.8	−477.94
2-methyl-1-butene	2-methyl-2-butene	−611.75	951.33
2-methyl-1-butene	*n*-pentane	326.74	−194.18
2-methyl-2-butene	methyl *tert*-pentyl ether	−386.04	712.33
2-methyl-2-butene	*n*-pentane	362.28	−265.49
methyl *tert*-pentyl ether	*n*-pentane	1143.9	−447.84

For the isomerization reaction we have

$$k_3 = 1078 \exp\left\{32.6 - \frac{10861}{T}\right\} \tag{61}$$

Bravo et al.[44] suggested the presence of multiple steady states in their pilot plant column for this process. Conclusive experimental evidence of multiple steady states in this process was described by Mohl et al.[1] In the following section we will take the configuration presented by Mohl et al. as a test case for our model. We model a packed column with an inner diameter of 0.076 m, consisting of two sections. The top section is 0.5-m high and packed with catalytic Raschig rings. The bottom section is 0.5-m high and packed with inert (glass) Raschig rings. A feed is supplied between the two sections. For more details about the column, see Mohl et al.[1]

The column pressure was 0.25 MPa and the reflux ratio 15. The feed consisted of methanol, the two pentenes, and inert *n*-pentane. The feed rate was 4.17 $\times 10^{-3}$ mol/s, with $x_{MeOH}/x_{C5=} = 0.8$ and $x_{C5=}/(x_{C5=} + x_{n\text{-}C5}) = 0.3$ using the information given by Mohl et al.[1] Sundmacher et al.[45] suggest that the Wilson equation should be used for describing nonideal liquid-phase behavior. Parameters for this model are given in Table 4.

Simulations were done with three different models: An equilibrium stage model with 12 stages and a stage efficiency of 0.8, a nonequilibrium model in which the reaction is assumed to be pseudohomogeneous, and a nonequilibrium model incorporating the dusty fluid model described here. For the nonequilibrium model, the packed section is divided into a number of slices, each considered to be a nonequilibrium cell. Calculations with the pseudohomogeneous model and 40 slices gave results that coincided with those obtained using only 10 slices; 10 slices were used in all subsequent calculations. It was further assumed that the column was packed with 1.3 kg of packing and that the catalyst activity was set to 1.2 equiv/kg.[1]

We have assumed the same catalyst geometry and properties as those for the MTBE problem. In addition, we have done calculations to determine the influence of the various geometrical parameters. In no case was there a significant influence of these parameters.

Three steady states were found for the base case column configuration. For obtaining the multiple steady states, a continuation method was used in which the reboiler duty was the independent parameter. Figure 8 shows the temperature profiles obtained for the high- and the low-production steady state, for the equilibrium model, for the nonequilibrium model with a pseudohomogeneous reaction, and for the nonequilibrium model with

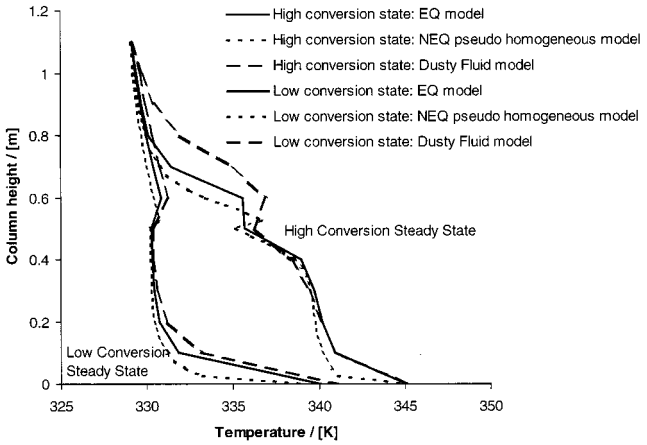

Figure 8. Temperature profiles for high- and low-conversion steady states in a TAME column for equilibrium (Eq), nonequilibrium (NQ), and dusty fluid (DF) models.

a dusty fluid description of the catalyst. All three models are largely in agreement with the calculated temperature profiles presented by Mohl et al.[1] and the differences between the models are minor. The same observation has been made by Sundmacher.[45] For this process, the overall conversion is not affected significantly by the mass-transfer resistance inside the porous catalyst.

5.3. Discussion. In the two case studies presented above we have found apparently contradictory findings. For the MTBE process, the differences between the equilibrium, pseudohomogeneous nonequilibrium, and dusty fluid nonequilibrium models are substantial. For the TAME process, all models give more or less similar results.

A reason for the difference must lie in the fact that the MTBE process is relatively sensitive to mass-transfer resistances, whereas the TAME process is not. There may be two reasons for this. First, for the TAME system, the entire catalytic section is used for the production of TAME both in the high- and the low-production steady states. In no case did we find consumption of TAME.

Second, the TAME reaction rate is much lower than that for the MTBE system. The forward reaction rate constant for TAME is about an order of magnitude lower than that for MTBE throughout the entire reactive section. The production rate of TAME will, therefore, be much less sensitive to changes in the mass-transfer resistance.

For the MTBE process there are substantial differences between equilibrium and nonequilibrium models.[21] In the equilibrium approach the reactive section is described by only 7 stages, whereas 90 slices were used in the nonequilibrium model calculations. The approximation of the real concentration and temperature profiles is, in the equilibrium stage model, much coarser than in the nonequilibrium model. The coarse prediction could give rise to significant deviations for systems with large temperature and concentration gradients in combination with highly nonlinear interactions between the reaction rates and the temperature profiles.

In addition, caution should be exercised in the application of efficiency factors for multiple steady-state calculations. Mohl et al.[1] describe calculations done with an equilibrium model, in which the value of the efficiency factor was fixed. However, one should keep in

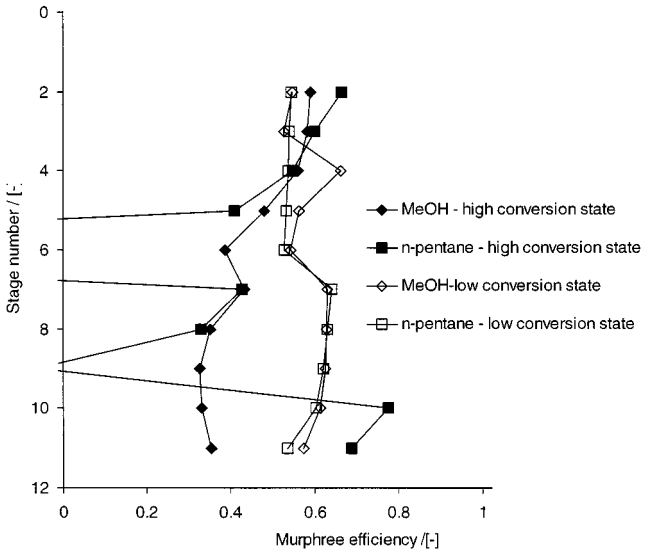

Figure 9. Murphree efficiency profiles for methanol and *n*-pentane at high- and low-conversion steady states.

mind that the hydrodynamic conditions in the various steady states may be quite different from each other, and so may the efficiencies. Figure 9. shows the Murphree efficiency profiles for methanol and *n*-pentane in the TAME column that were back-calculated from the results of the nonequilibrium dusty fluid model. As can be seen, the differences between the efficiencies in the high- and low-conversion steady states are quite considerable. Similar results are found for other components. The effect of the efficiencies on the overall conversion in the TAME process is not very large because the overall production rate is relatively insensitive to mass-transfer resistances. However, this will not always be the case.

6. Conclusions

We have described a nonequilibrium model for reactive distillation in porous catalysts. Important features of the model are the use of the Maxwell−Stefan theory for the description of interphase mass transfer and the use of the "dusty fluid model" for taking into account multicomponent mass transfer and reaction inside the porous catalyst.

The model was used to investigate the influence of the additional mass-transfer resistances that arise in and around the catalyst particles. Considerable differences between a nonequilibrium pseudohomogeneous model and a nonequilibrium dusty fluid model were found for the production of MTBE.

However, there were hardly any differences between a pseudohomogeneous nonequilibrium model and a dusty fluid nonequilibrium model for the production of TAME. In the TAME process the overall production rate does not depend on mass-transfer resistances (at least, in the range of parameter values studied here). The converse is true for the MTBE process. The rate of consumption of MTBE is very much influenced by additional mass-transfer resistances. This is in line with the observations reported by Higler et al.[21]

It should be remembered that a nonequilibrium model tries to describe a real column and, therefore, requires information about the column design and its internal configuration. This information is needed to calculate mass-transfer coefficients, interfacial areas, and so on.

The latter usually are obtained from semiempirical correlations. The computed solution of the model equations, therefore, depends to some extent on the quality of the correlations.

For the dusty fluid model, there are several model parameters for which good estimation methods are absent. First, there is a need for methods to estimate diffusion coefficients inside the catalyst. Diffusion coefficients can be concentration dependent and will, therefore, depend on the concentration and type of the catalyst. Second, there are no methods for evaluating nonideal thermodynamic behavior inside a catalyst.

Third, there is a need for correlations for the estimation of mass- and heat-transfer coefficients from the liquid bulk to the catalyst. This is particularly important for the newest generations of structured catalytic packing.

Acknowledgment

Partial support for our work is provided by BP−Amoco Chemicals and the members of the ChemSep consortium.

Notation

a = activity
a = interfacial area, m^2
a^C = catalyst surface area, m^2
$a_{i,j}$ = thermodynamic interaction parameters, $J \cdot mol^{-1}$
B_0 = permeability of porous medium, m^2
c = number of components
c_i = molar concentration of component i, $mol \cdot m^{-3}$
c_t = total concentration, $mol \cdot m^{-3}$
d_i = generalized driving force, m^{-1}
d_p = pore diameter, m
ϵ = energy-transfer rate, $J \cdot s^{-1}$
e^C = energy flux inside the catalyst, $J \cdot m^{-2} \cdot s^{-1}$
$Đ_{i,j}$ = Maxwell−Stefan diffusion coefficient, $m^2 \cdot s^{-1}$
D_i^e = Knudsen diffusion coefficient of component i, $m^2 \cdot s^{-1}$
F_i = external force acting per mole on species i, $N \cdot mol^{-1}$
H_k^L = liquid-phase enthalpy, $J \cdot mol^{-1}$
H_k^V = vapor-phase enthalpy, $J \cdot mol^{-1}$
H_i = partial molar enthalpy of component i, $J \cdot mol^{-1}$
h = heat-transfer coefficient, $J \cdot K^{-1} \cdot m^{-2} \cdot s^{-1}$
K_1, K_2, K_3 = chemical equilibrium constants
k_1, k_2, k_3 = reaction rate constants, $mol \cdot m^{-3} \cdot s^{-1}$
k^{LS} = liquid/solid mass-transfer coefficient, $m \cdot s^{-1}$
L_k = liquid flow rate from cell k, $mol \cdot s^{-1}$
L = characteristic length for diffusion, m
M_i = molar mass of species i, $kg \cdot mol^{-1}$
N_i = molar flux of component i, $mol \cdot m^{-2} \cdot s^{-1}$
N_i = mass-transfer rate of component i, $mol \cdot s^{-1}$
n_c = number of cells
n_s = number of stages
nr = number of reactions
n_1 = number of discretization points in liquid film at V/L interface
n_2 = number of discretization points in vapor film at V/L interface
n_3 = number of discretization points in liquid film at catalyst interface
n_4 = number of discretization points in catalyst
p = pressure, Pa
q = conductive heat flux, $J \cdot m^{-2} \cdot s^{-1}$
R_m = reaction rate of reaction m, $mol \cdot m^{-3} \cdot s^{-1}$
R = gas constant, $J \cdot mol^{-1} \cdot K^{-1}$
r_a = area ratio of mass-transfer film to catalyst surface area
r_1, r_2, r_3 = reaction rate, $mol \cdot m^{-3} \cdot s^{-1}$
T = temperature, K
u^L = superficial liquid velocity, $m \cdot s^{-1}$
$\bar{V}_i$ = molar volume, $m^3 \cdot mol^{-1}$
V_k = vapor flow rate from cell k, $mol \cdot s^{-1}$
V_C = catalyst volume in nonequilibrium cell, m^3
X = arbitrary variable
$x_{i,k}$ = liquid mole fraction of component i in cell k
$y_{i,k}$ = vapor mole fraction of component i in cell k
z_0 = distance from inner film surface to catalyst center, m
z_c = distance from catalyst surface to catalyst center, m
z_δ = distance from outer film surface to catalyst center, m

Greek Letters

α = power in eq 40
$\alpha_{i,j}$ = multicomponent thermal diffusion factor
β = power in eq 45
Γ = thermodynamic matrix
γ_i = activity coefficient of component i
$\delta_{i,j}$ = Kronecker delta, 1 if i = j, otherwise 0
ϵ = catalyst porosity
ϵ_k = volume fraction of catalyst in transfer film under consideration
η = dimensionless coordinate
η = viscosity, Pa.s
$\kappa_{i,j}$ = binary pair mass-transfer coefficient, $m \cdot s^{-1}$
λ = thermal conductivity, $J \cdot K^{-1} \cdot m^{-1} \cdot s^{-1}$
μ^i = chemical potential of component i, $J \cdot mol^{-1}$
$\nu_{i,m}$ = stoichiometric factor of component i in reaction m
ρ = liquid-phase density, $kg \cdot m^{-3}$
ϕ_i = volume fraction of component i
τ = catalyst tortuosity
ω_i = mass fraction of component i

Superscripts

$\sim$ = indicates pseudo quantity in dusty gas mixture
C = catalyst property or quantity
D = diffusive property
e = corrected for catalyst
L = liquid phase or liquid-transfer film at vapor/liquid interface
S = liquid-transfer film at liquid/solid interface
V = vapor-transfer film
V = viscous (in eqs 19−23)

Subscripts

2M1B = 2-methyl-1-butene
2M2B = 2-methyl-2-butene
C5= = pentene
i = component number index
k = cell number index
l = alternative component index
MeOH = methanol
n-C5 = pentane
t = total
TAME = *tert*-amyl methyl ether

Vector Notation

∇ = gradient operator, m^{-1}

Literature Cited

(1) Mohl, K. D.; Kienle, A.; Gilles. E. D.; Rapmund, P.; Sundmacher, K.; Hoffmann, U. Steady-State Multiplicities in Reactive Distillation Columns for the Production of Fuel Ethers Mtbe and Tame: Theoretical Analysis and Experimental Verification. *Chem. Eng. Sci.* **1999**, *54*, 1029.

(2) Seader, J. D.; Henley, E. J. *Separation Process Principles*; John Wiley: New York, 1998.

(3) Oudshoorn, O. L.; Janissen, M.; van Kooten, W. E. J.; Jansen, J. C.; van Bekkum, H.; van den Bleek, C. M.; Calis, H. P. A. A Novel Structured Catalyst Packing for Catalytic Distillation of ETBE. *Chem. Eng. Sci.* **1999**, *54*, 1413.

(4) Sundmacher, K.; Hoffmann, U. Multicomponent Mass and Energy Transport on Different Length Scales in a Packed Reactive Distillation Column for Heterogeneously Catalysed Fuel Ether Production. *Chem. Eng. Sci.* **1994**, *49*, 4443.

(5) Ellenberger, J.; Krishna, R. Counter-current Operation of a Structured Catalytically Packed Distillation Column: Pressure Drop, Holdup and Mixing. *Chem. Eng. Sci.* **1999**, *5*, 1339.

(6) Higler, A.; Krishna, R.; Ellenberger, J.; Taylor, R. Countercurrent Operation of a Structured Catalytically Packed Bed Reactor: Liquid Phase Mixing and Mass Transfer. *Chem. Eng. Sci.* **1999**, *54*, 5145.

(7) Xu, X.; Zheng, Y.; Zheng, G. Kinetics and Effectiveness of Catalyst for Synthesis of Methyl *tert*-butyl Ether in Catalytic Distillation. *Ind. Eng. Chem. Res.* **1995**, *34*, 2232.

(8) Davies, B.; Jenkins, J. D.; Dilfanian, S. Distillation with Chemical Reaction—The Distillation of Formaldehyde Solutions in a Sieve Plate Column. *Inst. Chem. Eng. Symp. Ser.* **1979**, *56*, 65.

(9) Barbosa, D.; Doherty, M. F. The Influence of Equilibrium Chemical Reactions on Vapor Liquid Phase Diagrams. *Chem. Eng. Sci.* **1988**, *43*, 529.

(10) Barbosa, D.; Doherty, M. F. The Simple Distillation of Homogeneous Reactive Mixtures. *Chem. Eng. Sci.* **1988**, *43*, 541.

(11) Carra, S.; Morbidelli, M.; Santacesaria, E.; Buzzi, G. Synthesis of Propylene Oxide from Propylene Chlorohydrins—II Modeling of the Distillation with Chemical Reaction Unit. *Chem. Eng. Sci.* **1979**, *34*, 1123.

(12) Alejski, K.; Szymanowski, J.; Bogacki, M. The Application of a Minimization Method for Solving Reactive Distillation Problems. *Comput. Chem. Eng.* **1988**, *12*, 833.

(13) Chang, Y. A.; Seader, J. D. Simulation of Continuous Reactive Distillation by a Homotopy Continuation Method. *Comput. Chem. Eng.* **1988**, *12*, 1234.

(14) Alejski, K. Computation of the Reacting Distillation Column Using a Liquid Mixing Model on the Plates. *Comput. Chem. Eng.* **1991**, *15*, 313.

(15) Simandl, J.; Svrcek, W. Y. Extension of the Simultaneous Solution and Inside Outside Algorithms to Distillation with Chemical Reactions. *Comput. Chem. Eng.* **1991**, *15*, 227.

(16) Ciric, A. R.; Gu, D. Synthesis of Nonequilibrium Reactive Distillation by MINLP Optimization. *AIChE J.* **1994**, *40*, 1479.

(17) Ciric, A. R.; Miao, P. Steady-State Multiplicities in an Ethylene Glycol Reactive Distillation Column. *Ind. Eng. Chem. Res.* **1994**, *33*, 2738.

(18) Abufares, A. A.; Douglas, P. L. Mathematical Modeling and Simulation of an MTBE Catalytic Distillation Process Using SpeedUp and AspenPlus. *Trans. Inst. Chem. Eng. A* **1995**, *73*, 3.

(19) Kreul, L. U.; Górak, A.; Barton, P. I. Modeling of Homogeneous Reactive Separation Processes in Packed Columns. *Chem. Eng. Sci.* **1999**, *54*, 19.

(20) Higler, A.; Krishna, R.; Taylor, R. A Nonequilibrium Cell Model for Multicomponent (Reactive) Separation Processes. *AIChE J.* **1999**, *45*, 2357.

(21) Higler, A.; Taylor, R.; Krishna, R. Nonequilibrium Modelling of Reactive Distillation: Multiple Steady States in MTBE Synthesis. *Chem. Eng. Sci.* **1999**, *54*, 1389.

(22) Krishnamurthy R.; Taylor, R. A Nonequilbrium Stage Model of Multicomponent Separation Processes, Part 1: Model Description and Method of Solution. *AIChE J.* **1985**, *3*, 449.

(23) Taylor, R.; Krishna, R. *Multicomponent Mass Transfer*; John Wiley: New York, 1993.

(24) Froment, G. F.; Bischoff, K. B. *Chemical Reactor Analysis and Design*, 2nd ed.; John Wiley: New York; 1990.

(25) Sundmacher, K.; Hoffmann, U. Importance of Irreversible Thermodynamics for Liquid-Phase Ion Exchange Catalysis: Experimental Verification for MTBE Synthesis. *Chem. Eng. Sci.* **1992**, *4*, 2733.

(26) Sundmacher, K.; Hoffmann, U. Macrokinetic Analysis of MTBE Synthesis in Chemical Potentials. *Chem. Eng. Sci.* **1994**, *49*, 3077.

(27) Krishna, R.; Wesselingh, J. A. The Maxwell-Stefan Approach to Mass Transfer. *Chem. Eng. Sci.* **1997**, *52*, 861.

(28) Maxwell, J. C. On the Dynamical Theory of Gases. *Philos. Trans. R. Soc.* **1866**, *157*, 49.

(29) Evans, R. B., III; Watson, G. M.; Mason, E. A. Gaseous Diffusion in Poroucs Media at Uniform Pressure. *J. Chem. Phys.* **1961**, *35*, 2076.

(30) Evans, R. B., III; Watson, G. M.; Mason, E. A. Gaseous Diffusion in Porous Media (II) Effect of Pressure Gradients. *J. Chem. Phys.* **1962**, *36*, 1894.

(31) Mason, E. A.; Evans, R. B., III; Watson, G. M. Gaseous Diffusion in porous Media (III) Thermal Transpiration. *J. Chem. Phys.* **1963**, *38*, 1808.

(32) Mason, E. A.; Malinauskas, A. P. Gaseous Diffusion in Porous Media (IV) Thermal Diffusion. *J. Chem. Phys.* **1964**, *4*, 3815.

(33) Mason, E. A.; Malinauskas, A. P.; Evans, R. B., III. Flow and Diffusion of Gases in Porous Media. *J. Chem. Phys.* **1964**, *41*, 3199.

(34) Jackson, R. *Transport in Porous Catalysts*; Elsevier: Amsterdam, 1977.

(35) Taylor, R.; Kooijman, H. A.; Hung, J.-S. A Second Generation Nonequilibrium Model for Computer Simulation of Multicomponent Separation Processes. *Comput. Chem. Eng.* **1994**, *18*, 205.

(36) Kooijman, H. A. Dynamic Nonequilibrium Column Simulation. Ph.D. Dissertation, Clarkson University, Potsdam, NY, 1995.

(37) Krevelen, D. W.; van Krekels, J. T. C. Rate of Dissolution of Solid Substances. *Recl. Trav. Chim. Pays-Bas.* **1948**, *14*, 1.

(38) Berg, D. A.; Harris, T. J. Characterisation of Multicomponent Diffusion Effects in MTBE Synthesis. *Ind. Eng. Chem. Res.* **1993**, *32*, 2147.

(39) Jacobs, R.; Krishna, R. Multiple Solutions in Reactive Distillation for Methyl *tert*-Butyl Ether Synthesis. *Ind. Eng. Chem. Res.* **1993**, *32*, 1706.

(40) Baur, R.; Higler, A. P.; Taylor, R.; Krishna, R. Comparison of Equilibrium Stage and Nonequilibrium Stage Models for Reactive Distillation. *Chem. Eng. J.* **1999**, *76*, 33.

(41) Oost, C.; Hoffmann, U. The Synthesis of Tertiary Amyl Ether (TAME): Microkinetics of the Reactions. *Chem. Eng. Sci.* **1995**, *51*, 329.

(42) Rihko, L.; Krause, A. D. Kinetics of the Heterogeneously Catalyzed *tert*-Amyl Methyl Ether Reactions in the Liquid Phase *Ind. Eng. Chem. Res.* **1995**, *34*, 1172.

(43) Thiel, C.; Sundmacher, K.; Hoffmann, U. Residue Curve Maps for Heterogeneously Catalysed Reactive Distillation of Fuel Ethers MTBE and TAME. *Chem. Eng. Sci.* **1997**, *52*, 993.

(44) Bravo, J. L.; Pyhalahti, A.; Järvelin, H. Investigations in a Catalytic Distillation Pilot Plant: Vapor/Liquid Equilibrium, Kinetics and Mass Transfer Issues. *Ind. Eng. Chem. Res.* **1993**, *32*, 2220.

(45) Sundmacher, K.; Uhde, G.; Hoffmann, U. Multiple Reactions in Catalytic Distillation Processes for the Production of the Fuel Oxygenates MTBE and TAME: Analysis by Rigorous Model and Experimental Validation. *Chem. Eng. Sci.* **1999**, *54*, 2839.

Received for review July 23, 1999
Revised manuscript received October 4, 1999
Accepted October 8, 1999

IE990547Q